

Microscopic electronic configurations after ultrafast magnetization dynamics

I. L. M. Locht,¹ I. Di Marco,¹ S. Garnerone,² A. Delin,^{1,3,4} and M. Battiato^{1,5,*}

¹*Dept. of Physics and Astronomy, Uppsala University, Box 516, SE-75120 Uppsala, Sweden*

²*Institute for Quantum Computing, University of Waterloo, Waterloo, Canada*

³*Department of Materials and Nanophysics, School of Information and Communication Technology, Electrum 229, Royal Institute of Technology (KTH), SE-16440 Kista, Sweden*

⁴*SeRC (Swedish e-Science Research Center), KTH, SE-10044 Stockholm, Sweden*

⁵*Institute of Solid State Physics, Vienna University of Technology, Vienna, Austria*

(Dated: April 6, 2022)

We provide a model for the prediction of the electronic and magnetic configurations of ferromagnetic Fe after an ultrafast decrease or increase of magnetization. The model is based on the well-grounded assumption that, after the ultrafast magnetization change, the system achieves a partial thermal equilibrium. With statistical arguments it is possible to show that the magnetic configurations are qualitatively different in the case of reduced or increased magnetization. The predicted magnetic configurations are then used to compute the dielectric response at the 3p (M) absorption edge, which can be related to the changes observed in the experimental T-MOKE data. The good qualitative agreement between theory and experiment offers a substantial support to the existence of an ultrafast increase of magnetisation, which has been fiercely debated in the last years.

PACS numbers: 75.78.Jp, 78.47.J-, 78.20.Ls, 05.70.Ln

The search for the next generation magnetic recording media is focusing on the ultrafast magnetization dynamics [1–5]. Despite experimental progress [6–15], the microscopic understanding of the ultrafast magnetization dynamics remains an open question. In the last few years, several theories were proposed as possible explanations [16–25], and are currently debated [26–34]. More recently the ultrafast build-up of magnetization in gold was measured [35], and ferromagnetic Fe was found to undergo both an ultrafast decrease or increase of magnetization [36]. In this last study, two different qualitative behaviours were observed in the experimental T-MOKE spectra at the 3p (M) absorption edge of Fe [36, 37]. For a demagnetized sample, the 3p asymmetry Fe peak is observed to decrease without noticeable changes of shape [36]. For a sample with increased magnetization, instead, the aforementioned peak remains approximately unaltered but a shoulder grows at lower transition energies [37], as shown in Fig. 1. While the decrease of a peak, even in the femtosecond timescale, has been already safely assigned to a net decrease of magnetisation, the growth of a shoulder is a new observation, which in Refs. 36 and 37 was associated to an increase of magnetization. However, this conjecture has not been fully accepted by the scientific community, and has fuelled a debate over the very existence of the ultrafast increase of magnetisation. Does the growth of the shoulder come from an increase of the Fe magnetization or from other effects, such as changes in the material response driven by a different element in the sample, or even by processes not involving magnetism? Answering these precise question is an important task to understand the existence of an ultrafast increase of magnetization, interpret experimental data, and possibly help in designing new experiments

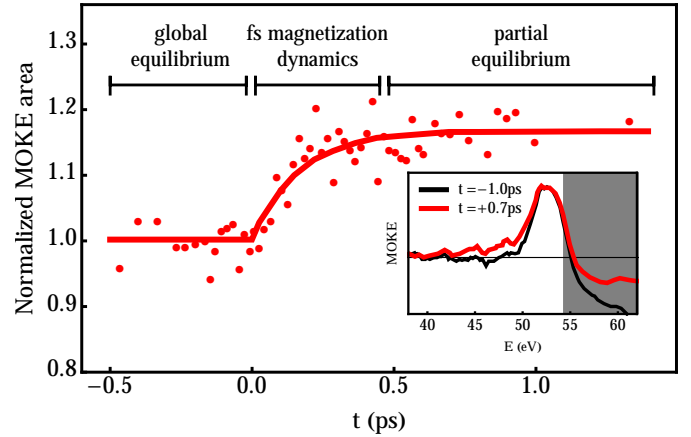


FIG. 1. [Colour online] Time-evolution of the area spanned by the 3p asymmetry Fe peak at 53 eV as reported in Ref. 37 for increased Fe magnetization. The relevant time-scales in the ultrafast magnetization dynamics in this experiment are also shown. In the inset the T-MOKE spectra at the M absorption edge are shown before (thin black line) and after (thick red line) the laser excitation, corresponding roughly to -1.0 ps and +0.7 ps.

and clarifying the very nature of the ultrafast dynamics.

The aim of the present paper is to provide a model to describe the excited states of Fe after ultrafast magnetization dynamics, and predict the magnetic response of the material. We will address the decrease and increase of magnetization on equal footing. We will show that the system has acquired a partial thermal equilibrium in the picosecond time-scale. This partial equilibrium will be described using microcanonical statistics on a subspace of the whole Hilbert space. Ensemble averages will show that the two resulting magnetic config-

urations, described in terms of local atomic moments, are qualitatively different in microscopic sense. After ultrafast demagnetization, the system is found to have tilted atomic magnetic moments whose lengths are equal to the equilibrium value. On the contrary, after ultrafast magnetization increase, the magnetic configuration is given by aligned atomic magnetic moments with increased lengths. Dielectric tensors are finally computed for the predicted magnetic configurations, and show the same features observed in the experimentally measured asymmetry. This offers a strong support to the existence of an ultrafast increase of magnetization in Fe.

Let us consider a sample of Fe after an ultrafast change of magnetization, as in Ref. 36. Our first step consists in defining an unambiguous characterization of all possible states of the system at a microscopic level. We call these states microstates. Note that the ground state of the system is one microstate (see point A in Fig. 2), while the other microstates are all possible excited states (see as examples points B and C in Fig. 2). We first characterize a microstate by its magnetic configuration (\mathbf{m}_i), representing the length and orientation of the local magnetic moments on each atom i . Note that even in an itinerant ferromagnet like Fe, the d bands remain fairly localized around each nucleus and an atomic magnetic moment can be defined with very good approximation [38]. Providing the magnetic configuration (\mathbf{m}_i) alone does not univocally define the microstate, since the energy configuration of the electrons has to be provided as well. This requires a characterization of the electronic excitations, which we describe as superpositions of single electron promotions on the rigid band structure. The latter is obtained from the microstate that is compatible with the given magnetic configuration and has the lowest energy. We fully describe the electronic configuration of the microstate by specifying the electronic population of the density of states. Note that all possible repopulations that do not alter the total number of majority and minority spin electrons give all microstates compatible with the magnetic configuration. This description of the excited states is fairly good in metals, provided that correlation effects are not too strong. This is indeed the case for Fe, as emphasized by recent dynamical mean-field theory (DMFT) calculations [39]. However, we stress that all the conclusions reached throughout the paper hold irrespectively of the description of the excited states, and this approximate analysis is provided with the only purpose of making the arguments below less abstract and more intuitive. In our analysis a microstate is thus defined by its magnetic configuration and its electronic configuration.

Once the microstates have been classified, we can identify the subspace of partial equilibration. The system explores the space of allowed microstates via electron-electron (e-e) scattering. For simplicity, we neglect electron-phonon scattering, but its inclusion would lead

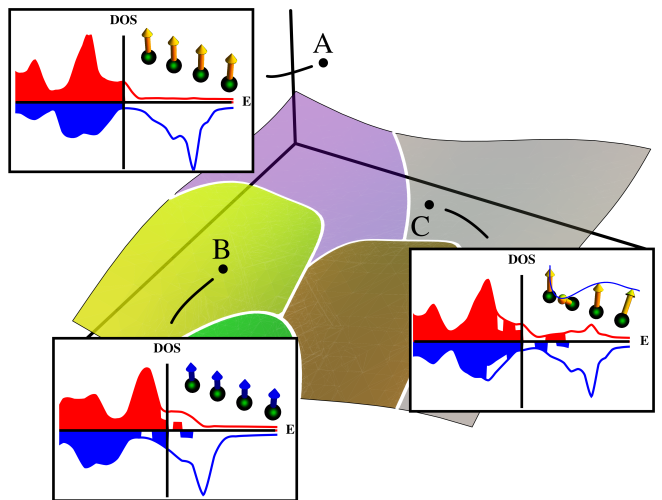


FIG. 2. [Colour online] Pictorial view of the possible microstates in the Hilbert space. The surface represents the subspace satisfying the constraints of fixed energy and fixed magnetization. The colored regions represent subspaces with different magnetic configurations. As examples, in addition to the ground state of point A, two microstates are shown, belonging to two areas with different magnetic configurations. Point B is a microstate with atomic magnetic moments reduced in amplitude and aligned. Point C is a microstate with magnetic moments with equilibrium length but disordered direction. The insets show the density of states for both majority (red, top) and minority (blue, bottom) spins, together with a cartoon of the orientation and length of the atomic magnetic moments. The arrows are coloured according to their length, as in Fig. 3.

to, and indeed strengthen, the same conclusions [40]. The main effect of the e-e scattering is the reshuffling of the energy positions of the electrons without changing the total energy of the system. The spin-orbit coupling for 3d-levels in Fe is small, which leads to a small probability to transfer spin moment to the lattice. Therefore, in the picosecond time scale, the majority of e-e scattering events preserve both the total energy E_{tot} and magnetization M_{tot} (both defined as renormalized with respect to the number of atoms N_{at} in the system). Consequently the change of total spin moment can be regarded as a quasi-static process compared to the exploration of the subspace due to energy- and magnetization-conserving e-e scattering events [40]. These can still lead to the transition from one microstate with a given magnetic configuration (\mathbf{m}_i) to another with a different one (\mathbf{m}'_i), as long as the total moment is preserved, i.e. $\sum_{i=1}^{N_{\text{at}}} \mathbf{m}_i / N_{\text{at}} = \sum_{i=1}^{N_{\text{at}}} \mathbf{m}'_i / N_{\text{at}}$. This situation is for instance represented by the two microstates B and C in Fig. 2. Moreover, experiments show that, about a ps after the laser excitation, the electrons acquire a Fermi-Dirac distribution, characterized by an effective high temperature [41, 42]. We use this experimental fact, whose the-

oretical analysis follows this paragraph, to assume that the electronic system is in a partial thermal equilibrium. The partial attribute is due to that this system still has a total magnetization M_{tot} which is different (higher or lower) than the global equilibrium value at a specific temperature. In summary, the e-e scattering allows the system to effectively equilibrate in the subspace including all possible electronic arrangements under two constraints. These are a fixed total energy E_{tot} (set by the energy deposited by the laser) and a fixed total magnetic moment M_{tot} (set by the mechanism responsible for the ultrafast magnetization dynamics). Notice that our model is independent of the specific mechanisms driving the ultrafast dynamics, but the value of M_{tot} is set by this transient process, and is therefore dependent on it [40].

From a more theoretical point of view, the mechanism allowing isolated macroscopic quantum systems to equilibrate, the time-scales involved in this process, and the details of the approach to effective ergodicity, are under intense study [43–48]. For instance, it has been argued that standard ergodicity (i.e. the identification between time and ensemble averages), given the large dimension of the Hilbert space, is not a viable mechanism to explain equilibration in isolated macroscopic quantum systems. Following a forgotten intuition by Von Neumann [44], the relevant mechanism has been suggested to be the normal typicality, which is based on the most common instantaneous behaviour of the system. In particular, it has been shown that, for the vast majority of isolated (negligible interaction with the environment) quantum dynamics and for the vast majority of time instants, the microscopic state of the system is practically indistinguishable from, i.e. *macroscopically equivalent* to, the equilibrium state [44].

The subspace of partial equilibration can now be used to evaluate the expectation value of any observable as an ensemble average. In particular we want to compute the average magnetic configuration, which, due to the macroscopical equivalence discussed above, is negligibly different from the most probable one. The most probable magnetic configuration is the one corresponding to the largest partition of the Hilbert space [44], i.e associated with the highest number of microstates or equivalently the maximum of the entropy. For a fermionic system with a constant density of states ρ , the number of ways \mathcal{N} to arrange the electronic excitations as a function of the energy E_{tot} can be calculated in the degenerate gas approximation [49]. This formula can be directly generalized to two different spin populations, and to a system partitioned in terms of local moments and local densities of states, leading to

$$\mathcal{N} \propto e^{N_{\text{at}} \sqrt{\bar{\rho}[\mathbf{m}_i] (E_{\text{tot}} - E_{\text{min}}[\mathbf{m}_i])}} \quad (1)$$

where E_{min} is the energy of the fermionic magnetic ground state and $\bar{\rho}$ is the average on both spin channels

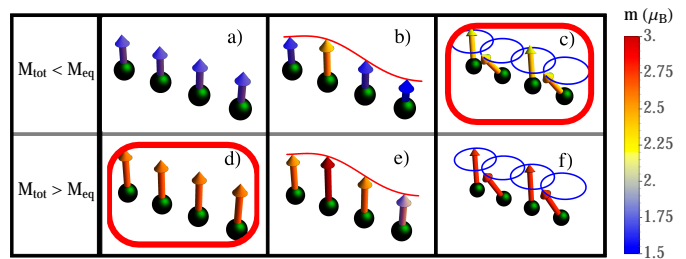


FIG. 3. [Colour online] The top panels show some possible magnetic configurations with a decreased average magnetic moment. In the bottom panels the same type of configurations are shown for an increased average magnetic moment. From left to right: a linear decrease or increase, amplitude spin fluctuations, transverse spin fluctuations. The arrows are coloured according to their length.

of the density of states over an energy range comparable to $E_{\text{tot}} - E_{\text{min}}$. Since N_{at} is proportional to the Avogadro number, any increase of the product $\bar{\rho}[\mathbf{m}_i] (E_{\text{tot}} - E_{\text{min}}[\mathbf{m}_i])$ will produce an enormous increase on the possible electronic arrangements. The most probable configuration is the one that maximises the exponent in Eq. 1, or more simply the one with the lowest $E_{\text{min}}[\mathbf{m}_i]$, as we will see below.

We first identify all the possible magnetic configurations (\mathbf{m}_i) satisfying the constraint on the total magnetic moment $|\sum_{i=1}^{N_{\text{at}}} \mathbf{m}_i / N_{\text{at}}| = M_{\text{tot}}$. The second step will be to calculate $\bar{\rho}[\mathbf{m}_i]$ and $(E_{\text{tot}} - E_{\text{min}}[\mathbf{m}_i])$ for these magnetic configurations. In Fig. 3 we show examples of possible magnetic configurations. The density of states $\rho[\mathbf{m}_i]$ for the configurations in Fig. 3a and Fig. 3d can be computed directly through constrained density functional theory (DFT) [50] with fixed spin moments (\mathbf{m}_i). We find that $\bar{\rho}[\mathbf{m}_i]$ is approximately constant [40, 51, 52]. Therefore, maximizing the product $\bar{\rho}[\mathbf{m}_i] (E_{\text{tot}} - E_{\text{min}}[\mathbf{m}_i])$ implies minimizing $E_{\text{min}}[\mathbf{m}_i]$, which is instead strongly dependent on the magnetic configuration.

The values $E_{\text{min}}[\mathbf{m}_i]$ for ferromagnetic configurations as in Fig. 3a and Fig. 3d are reported in Fig. 4 as obtained from DFT [40]. The $E_{\text{min}}[\mathbf{m}_i]$ for magnetic configurations as in Fig. 3c and Fig. 3f can be obtained by calculating the energy of magnon modes [53]. With these values, we can show that in case of decreased magnetization $M_{\text{tot}} < M_{\text{eq}}$, the magnetic configuration (\mathbf{m}_i) with the lowest $E_{\text{min}}[\mathbf{m}_i]$ (and therefore the most probable one) is the one shown in Fig. 3c, where the atomic moments retain their equilibrium length but are tilted with a small wave-vector \mathbf{q} . Contrarily in the case of increased magnetization $M_{\text{tot}} > M_{\text{eq}}$, the atomic moments are aligned and have an increased length, as shown in Fig. 3d. Above and in the figures we have labeled as M_{eq} the ferromagnetic equilibrium value of the Fe magnetization at the temperature of the experiment, i.e. about $2.2 \mu_B$.

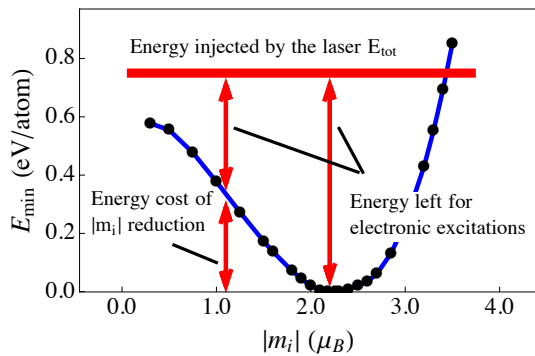


FIG. 4. [Colour online] Constrained ground state energy for ferromagnetic configurations as in Fig. 3a and Fig. 3d as function of the atomic magnetic moment $|m_i|$ (the index i is unimportant here). The zero of the energy is defined by the equilibrium atomic magnetic moment. The energy deposited by the laser is drawn schematically, and exaggerated for clarity, to emphasize what energy is left available for electronic excitations.

The reason for two qualitatively different minima is easy to understand in our model. For reduced magnetization, the minimum energy compatible with the ferromagnetic configuration in Fig. 3a is given by the cost associated to the reduction of the length of the atomic moments ($|m_i|$), as shown in Fig. 4. This is basically the intra-site exchange. On the other hand the magnetic configuration in Fig. 3c has an energy cost depending on both the inter-site exchange and the magnetic anisotropy energy. The anisotropy in Fe is small compared to the exchange [54], and can be ignored here. The energy price for the inter-site exchange is minimized for fluctuations with a small wave-vector, and is significantly lower than the cost due to intra-site exchange. A rather different situation is observed for increased magnetization. The configuration in Fig. 3d has a high E_{\min} because of the energy needed to increase the atomic magnetic moments. However, the configuration in Fig. 3f has an even higher E_{\min} because the atomic moments, when tilted, need to be even bigger to achieve the required M_{tot} .

Now that the largest partition of the Hilbert space has been determined, we can compute the dielectric response. As mentioned above, all macroscopic characteristics of a quantum system at equilibrium are at almost every time indistinguishable from the microcanonical ensemble averages, corresponding here to expectation values obtained with the most probable occupations of the single-particle energy levels, i.e. the Fermi-Dirac distribution. We used the DFT simulations to calculate the optical conductivity tensor [40, 51, 52, 55]. We are mainly interested in the off-diagonal term ϵ_{xy} , which is approximately proportional to the experimental T-MOKE asymmetry, for a system with cubic symmetry and magnetisation along the z direction. Since the local band structure is almost unchanged, and the atomic magnetic moments are just

tilted with respect to the light incidence and polarization, ϵ_{xy} is (approximately) reduced without distortion [40]. This is illustrated in the lower part of Fig. 5. Instead, the configuration with increased magnetization consists of increased atomic magnetic moments, which leads to an increased population of the spin majority band and a reduction of the population of the spin minority band. This induces a change in the density of states above the Fermi energy and an increase of the spin splitting of the core levels. As a result, the dielectric response changes only below 52 eV, as highlighted within the red boxes in Fig. 5. This compares qualitatively well with the fact that the experimental T-MOKE is modified only at energies below the main Fe peak.

The good agreement between theoretical and experimental features across several magnetizations gives a solid theoretical background to the hypothesis made in Refs. 36 and 37 that the change of the area spanned by the T-MOKE Fe peak is related to the change in the magnetization itself, even when due to the growth of a shoulder. Determining the exact quantitative relation between area and magnetization would require a complete calculation of the T-MOKE asymmetry, and will be object of our future research. Note that our results for the demagnetized sample are in principle obtainable also by static magneto-optical approaches, as done by Carva *et al.* [56] for a few trial electronic configurations. No such analogy exists, instead, for the case of increased magnetization. However, we stress once more that our model does not explore a few trial configurations, but aims at the very prediction of the microscopic state to investigate. This problem was never addressed before. It is also interesting that the microscopic state predicted by our model for the demagnetized case is not included in the trial configurations of Ref. 56.

In conclusion, we provided a solid theoretical description of the microscopic states of a system right after ultrafast magnetization dynamics. This is of great importance for the study of the picosecond dynamics of magnetization, when the system is in an out-of-equilibrium state but the magnetic dynamics can be treated as a quasi-static evolution of a partially equilibrated system. The dielectric response can be computed by means of well-grounded approximations, and show a good qualitative agreement with the available experimental data. In addition, the proposed method can be applied to more general situations, e.g the case of magnetized gold [35]. We will also address the dielectric response of Ru with a transient magnetic moment for computing the T-MOKE asymmetry measured experimentally [36]. Finally, the treatment can be extended to more complex materials, and even to the case of two magnetic subsystems that are internally but not mutually equilibrated, e.g. d and f states for Gd [7, 14] or the different sub-lattices in the alloys used for all-optical switching [3, 10].

This work was sponsored by the Swedish Research

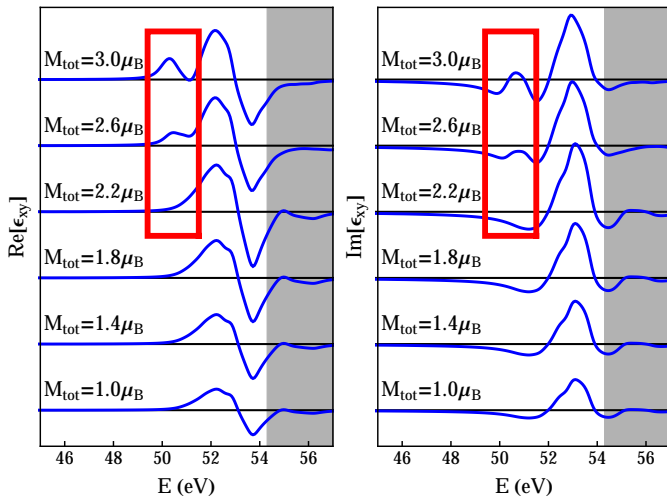


FIG. 5. [Colour online] Real and imaginary parts of the off-diagonal term of the dielectric tensor for decreased and increased magnetisations. The shaded grey area identifies those energies where the T-MOKE signals of Fe and Ni overlap, making any comparison with experimental data [36, 37] not meaningful. For increased magnetization a shoulder in the Fe peak is formed, as highlighted within the red box.

Council (VR), the Royal Swedish Academy of Sciences (KVA), and the Knut and Alice Wallenberg foundation (KAW). The computations were performed on resources provided by the Swedish National Infrastructure for Computing (SNIC) at the National Supercomputer Center (NSC). The authors thank D. Rudolf, R. Chimata, O. Eriksson, and J. Rusz for valuable discussions.

* marco.battiato@ifp.tuwien.ac.at

- [1] E. Beaurepaire, J. C. Merle, A. Daunois, and J.-Y. Bigot, *Phys. Rev. Lett.* **76**, 4250 (1996).
- [2] A. Kirilyuk, A. V. Kimel, and T. Rasing, *Rev. Mod. Phys.* **82**, 2731 (2010).
- [3] C. D. Stanciu, F. Hansteen, A. V. Kimel, A. Kirilyuk, A. Tsukamoto, A. Itoh, and T. Rasing, *Phys. Rev. Lett.* **99**, 047601 (2007).
- [4] G. Malinowski, F. Dalla Longa, J. H. H. Rietjens, P. V. Paluskar, R. Huijink, H. J. M. Swagten, and B. Koopmans, *Nature Phys.* **4**, 855 (2008).
- [5] K. Vahaplar, A. M. Kalashnikova, A. V. Kimel, D. Hinzke, U. Nowak, R. Chantrell, A. Tsukamoto, A. Itoh, A. Kirilyuk, and T. Rasing, *Phys. Rev. Lett.* **103**, 117201 (2009).
- [6] C. Stamm, T. Kachel, N. Pontius, R. Mitzner, T. Quast, K. Holldack, S. Khan, C. Lupulescu, E. F. Aziz, M. Wietstruk, H. A. Dürr, and W. Eberhardt, *Nature Mater.* **6**, 740 (2007).
- [7] A. Melnikov, H. Prima-Garcia, M. Lisowski, T. Gießel, R. Weber, R. Schmidt, C. Gahl, N. M. Bulgakova, U. Bovensiepen, and M. Weinelt, *Phys. Rev. Lett.* **100**, 107202 (2008).
- [8] G. M. Müller, J. Walowski, M. Djordjevic, G.-X. Miao, A. Gupta, A. V. Ramos, K. Gehrke, V. Moshnyaga, K. Samwer, J. Schmalhorst, A. Thomas, A. Huettner, G. Reiss, J. S. Moodera, and M. Münzenberg, *Nature Mater.* **8**, 56 (2009).
- [9] J.-Y. Bigot, M. Vomir, and E. Beaurepaire, *Nature Phys.* **5**, 515 (2009).
- [10] I. Radu, K. Vahaplar, C. Stamm, T. Kachel, N. Pontius, H. A. Dürr, T. A. Ostler, J. Barker, R. F. L. Evans, R. W. Chantrell, A. Tsukamoto, A. Itoh, A. Kirilyuk, T. Rasing, and A. V. Kimel, *Nature* **472**, 205 (2011).
- [11] C. La-O-Vorakiat, E. Turgut, C. A. Teale, H. C. Kapteyn, M. M. Murnane, S. Mathias, M. Aeschlimann, C. M. Schneider, J. M. Shaw, H. T. Nembach, and T. J. Silva, *Phys. Rev. X* **2**, 011005 (2012).
- [12] S. Mathias, C. La-O-Vorakiat, P. Grychtol, P. Granitzka, E. Turgut, J. M. Shaw, R. Adam, H. T. Nembach, M. E. Siemens, S. Eich, C. M. Schneider, T. J. Silva, M. Aeschlimann, M. M. Murnane, and H. C. Kapteyn, *Proc. Natl. Acad. Sci. USA* **109**, 4792 (2012).
- [13] T. A. Ostler, J. Barker, R. F. L. Evans, R. W. Chantrell, U. Atxitia, O. Chubykalo-Fesenko, S. El Moussaoui, L. Le Guyader, E. Mengotti, L. J. Heyderman, F. Nolting, A. Tsukamoto, A. Itoh, D. Afanasiev, B. A. Ivanov, A. M. Kalashnikova, K. Vahaplar, J. Mentink, A. Kirilyuk, T. Rasing, and A. V. Kimel, *Nature Commun.* **3**, 666 (2012).
- [14] R. Carley, K. Döbrich, B. Frietsch, C. Gahl, M. Teichmann, O. Schwarzkopf, P. Wernet, and M. Weinelt, *Phys. Rev. Lett.* **109**, 057401 (2012).
- [15] T. Kampfrath, M. Battiato, P. Maldonado, G. Eilers, J. Notzold, S. Mahrlein, V. Zbarsky, F. Freimuth, Y. Mokrousov, S. Blügel, M. Wolf, I. Radu, P. M. Oppeneer, and M. Münzenberg, *Nature Nanotechn.* **8**, 256 (2013).
- [16] B. Koopmans, J. J. M. Ruigrok, F. Dalla Longa, and W. J. M. de Jonge, *Phys. Rev. Lett.* **95**, 267207 (2005).
- [17] E. Carpene, E. Mancini, C. Dallera, M. Brenna, E. Puppin, and S. De Silvestri, *Phys. Rev. B* **78**, 174422 (2008).
- [18] M. Krauss, T. Roth, S. Alebrand, D. Steil, M. Cinchetti, M. Aeschlimann, and H. C. Schneider, *Phys. Rev. B* **80**, 180407(R) (2009).
- [19] G. P. Zhang, W. Hübner, G. Lefkidis, Y. Bai, and T. F. George, *Nature Phys.* **5**, 499 (2009).
- [20] B. Koopmans, G. Malinowski, F. Dalla Longa, D. Steiauf, M. Faehle, T. Roth, M. Cinchetti, and M. Aeschlimann, *Nature Mater.* **9**, 259 (2010).
- [21] R. Chimata, A. Bergman, L. Bergqvist, B. Sanyal, and O. Eriksson, *Phys. Rev. Lett.* **109**, 157201 (2012).
- [22] M. Battiato, K. Carva, and P. M. Oppeneer, *Phys. Rev. Lett.* **105**, 027203 (2010).
- [23] M. Battiato, K. Carva, and P. M. Oppeneer, *Phys. Rev. B* **86**, 024404 (2012).
- [24] M. Battiato, P. Maldonado, and P. M. Oppeneer, *J. Appl. Phys.* **115**, 172611 (2014).
- [25] S. Wienholdt, D. Hinzke, K. Carva, P. M. Oppeneer, and U. Nowak, *Phys. Rev. B* **88**, 020406 (2013).
- [26] K. Carva, M. Battiato, and P. M. Oppeneer, *Nature Phys.* **7**, 665 (2011).
- [27] K. Carva, M. Battiato, and P. M. Oppeneer, *Phys. Rev. Lett.* **107**, 207201 (2011).
- [28] K. Carva, M. Battiato, D. Legut, and P. M. Oppeneer, *Phys. Rev. B* **87**, 184425 (2013).
- [29] A. Eschenlohr, M. Battiato, P. Maldonado, N. Pontius,

- T. Kachel, K. Holldack, R. Mitzner, A. Föhlich, P. M. Oppeneer, and C. Stamm, *Nature Mater.* **12**, 332 (2013).
- [30] C. E. Graves, A. H. Reid, T. Wang, B. Wu, S. de Jong, K. Vahaplar, I. Radu, D. P. Bernstein, M. Messerschmidt, L. Müller, R. Coffee, M. Bionta, S. W. Epp, R. Hartmann, N. Kimmel, G. Hauser, A. Hartmann, P. Holl, H. Gorke, J. H. Mentink, A. Tsukamoto, A. Fognini, J. J. Turner, W. F. Schlotter, D. Rolles, H. Soltau, L. Strüder, Y. Acremann, A. V. Kimel, A. Kirilyuk, T. Rasing, J. Stöhr, A. O. Scherz, and H. A. Dürr, *Nature Mater.* **12**, 293 (2013).
- [31] B. Vodungbo, J. Gautier, G. Lambert, A. B. Sardinha, M. Lozano, S. Sebban, M. Ducouso, W. Boutu, K. Li, B. Tudu, M. Tortarolo, R. Hawaldar, R. Delaunay, V. López-Flores, J. Arabski, C. Boeglin, H. Merdji, P. Zeitoun, and J. Lüning, *Nature Commun.* **3**, 999 (2012).
- [32] B. Pfau, S. Schaffert, L. Müller, C. Gutt, A. Al-Shemmary, F. Büttner, R. Delaunay, S. Düsterer, S. Flewett, R. Frömter, J. Geilhufe, E. Guehrs, C. M. Günther, R. Hawaldar, M. Hille, N. Jaouen, A. Kobs, K. Li, J. Mohanty, H. Redlin, W. F. Schlotter, D. Stickler, R. Treusch, B. Vodungbo, M. Kläui, H. P. Oepen, J. Lüning, G. Grübel, and S. Eisebitt, *Nature Commun.* **3**, 1100 (2012).
- [33] A. J. Schellekens and B. Koopmans, *Phys. Rev. Lett.* **110**, 217204 (2013).
- [34] W. He, T. Zhu, X.-Q. Zhang, H.-T. Yang, and Z.-H. Cheng, *Sci. Rep.* **3** (2013).
- [35] A. Melnikov, I. Razdolski, T. O. Wehling, E. T. Papaioannou, V. Roddatis, P. Fumagalli, O. Aktsipetrov, A. I. Lichtenstein, and U. Bovensiepen, *Phys. Rev. Lett.* **107**, 076601 (2011).
- [36] D. Rudolf, C. La-O-Vorakiat, M. Battiato, R. Adam, J. M. Shaw, E. Turgut, P. Maldonado, S. Mathias, P. Grychtol, H. T. Nembach, T. J. Silva, M. Aeschlimann, H. C. Kapteyn, M. M. Murnane, C. M. Schneider, and P. M. Oppeneer, *Nature Commun.* **3**, 1037 (2012).
- [37] E. Turgut, C. La-o-vorakiat, J. M. Shaw, P. Grychtol, H. T. Nembach, D. Rudolf, R. Adam, M. Aeschlimann, C. M. Schneider, T. J. Silva, M. M. Murnane, H. C. Kapteyn, and S. Mathias, *Phys. Rev. Lett.* **110**, 197201 (2013).
- [38] N. M. Rosengaard and B. Johansson, *Phys. Rev. B* **55**, 14975 (1997).
- [39] J. Sánchez-Barriga, J. Fink, V. Boni, I. Di Marco, J. Braun, J. Minár, A. Varykhalov, O. Rader, V. Bellini, F. Manghi, H. Ebert, M. I. Katsnelson, A. I. Lichtenstein, O. Eriksson, W. Eberhardt, and H. A. Dürr, *Phys. Rev. Lett.* **103**, 267203 (2009).
- [40] See Supplemental Material for a full account of the computational details and other additional information.
- [41] M. Lisowski, P. A. Loukakos, U. Bovensiepen, J. Stahler, C. Gahl, and M. Wolf, *Appl. Phys. A-Mater.* **78**, 165 (2004).
- [42] M. Lisowski, P. A. Loukakos, A. Melnikov, I. Radu, L. Ungureanu, M. Wolf, and U. Bovensiepen, *Phys. Rev. Lett.* **95**, 137402 (2005).
- [43] M. Rigol, V. Dunjko, and M. Olshanii, *Nature* **452**, 854 (2008).
- [44] S. Goldstein, J. L. Lebowitz, C. Mastrodonato, R. Tumulka, and N. Zanghi, *Proceedings of the Royal Society A: Mathematical, Physical and Engineering Science* **466**, 3203 (2010).
- [45] S. Goldstein, J. L. Lebowitz, R. Tumulka, and N. Zanghi, *Phys. Rev. Lett.* **96**, 050403 (2006).
- [46] S. Goldstein, T. Hara, and H. Tasaki, *Phys. Rev. Lett.* **111**, 140401 (2013).
- [47] S. Garnerone, T. R. de Oliveira, and P. Zanardi, *Phys. Rev. A* **81**, 032336 (2010).
- [48] S. Garnerone, *Phys. Rev. B* **88**, 165140 (2013).
- [49] J. Roccia and P. Leboeuf, *Phys. Rev. C* **81**, 044301 (2010).
- [50] P. H. Dederichs, S. Blügel, R. Zeller, and H. Akai, *Phys. Rev. Lett.* **53**, 2512 (1984).
- [51] <http://elk.sourceforge.net/>.
- [52] J. P. Perdew, K. Burke, and M. Ernzerhof, *Phys. Rev. Lett.* **77**, 3865 (1996).
- [53] J. K. Kübler, *Theory of itinerant electron magnetism* (Oxford University Press, Oxford, 2009).
- [54] M. Stearns, in *3d, 4d and 5d Elements, Alloys and Compounds*, Landolt-Börnstein - Group III Condensed Matter, Vol. 19a, edited by H. Wijn (Springer Berlin Heidelberg, 1986) pp. 41–47.
- [55] H. Rathgen and M. I. Katsnelson, *Physica Scripta* **2004**, 170 (2004).
- [56] K. Carva, D. Legut, and P. M. Oppeneer, *EPL* **86** (2009).

Supplemental Material: Microscopic electronic configurations after ultrafast magnetisation dynamics

Clarifying remark on the Hilbert space and the philosophy of the treatment of different timescales. Technical information about the computation of the number of configurations, the role of the electron-phonon scattering, the first-principles simulations, and the rotations of the dielectric tensor.

REMARK ON THE HILBERT SPACE

Throughout our manuscript we often talk of microcanonical statistics on a subspace of the whole Hilbert space. In classical terms we would talk here of the phase space of the dynamical system of the 10^{23} electrons composing the solid. However, in quantum statistical mechanics, the phase space does not exist, due to the Heisenberg uncertainty principle, and therefore we talk more generically of a Hilbert space.

SEPARATION OF TIMESCALES

We have addressed in the article two timescales and treated them differently. Here we clarify the distinction. The ultrafast change of magnetisation happens in the first few hundred femtoseconds. For shortness, we name these processes sub-picosecond dynamics. Similarly we name the dynamics happening in the picosecond timescale as picosecond dynamics. The reader has to anyhow be aware that the precise timescale obviously depends on the material under consideration and the sample configuration.

In the analysis of the sub-picosecond timescale we suppose that all the processes that happen on the picosecond timescale are negligible during the sub-picosecond one. In the article we address this timescale by showing that the state of the system at the end of the sub-picosecond dynamics depends only on two parameters: the average magnetisation and the total energy of the system. The fact that the state of the system does not depend on the details of the ultrafast process is a fundamental step in understanding the spectral response of the system. A knowledge of the sub-picosecond process is anyhow in principle still needed to extract those two values. Nonetheless in this work we do not address the exact calculation of these parameters and predict the state of the system for all the possible values.

After the ultrafast change of magnetization has finished, the processes in the picosecond time scale become important. During this timescale the system undergoes different dynamics: cooling down due to heat diffusion, recovery of the magnetic moment due to the slow spin-phonon equilibration, and precession of the atomic magnetic moments in the magnetic field. The first two processes (cooling and recovery of magnetisation) can be treated as quasi static, and therefore can be excluded from the calculation of the state at 500 fs and thereafter. For this reason they influence the state of the system only by setting the time dependence of $M_{\text{tot}}(t)$ and $E_{\text{tot}}(t)$. The precession of the atomic magnetic moments, instead, leads to magnonic oscillations, which points towards a Landau-Lifshitz evolution with parameters that can be computed for the partially equilibrated state rather than for the completely equilibrated one. The description of these processes is way beyond the scope of our work. The latter dynamics will anyhow not influence the spectrum. Notice finally that our theory can be considered as a probe of the microscopic state at any given time t in the picosecond regime.

NUMBER OF CONFIGURATIONS

For reader's convenience we report here the derivation of Eq. 1 in the main paper. This equation, and the following derivation, are limited to the particular case of a fermionic system with a constant density of states, and are reported only for illustrative purposes. A more general case is analyzed elsewhere [49], and we redirect the reader to this work for all the details. We start computing the grand canonical partition function for non interacting electrons over a constant single particle density of states. To simplify our derivation we assume this density of states to be finite only above 0, so that it has effectively the form of a step function. This assumption has no consequence on the results but makes it possible to have a much easier mathematical treatment of the interval of integration.

We first derive the expression for the discrete case of equally spaced energy levels, and we will then take the continuous limit as $N_{\text{at}} \rightarrow \infty$, where N_{at} can be interpreted as the number of atoms. The discrete energy levels for one atom are defined as $E_j = j \delta E_1$, with j being a generic quantum number going from one till infinity, and are

characterized by the occupation numbers $n_j = 0, 1$. When going to the many atoms case, the splitting between the levels must be adjusted to be inversely proportional to the number of atoms in the system, i.e. $\delta E_{N_{\text{at}}} = \delta E_1 / N_{\text{at}}$. It is easy to see that in the continuous limit the total density of states $D_{N_{\text{at}}} = 1 / \delta E_{N_{\text{at}}}$ grows to infinity but the density of states per unit cell remains constant $\rho = D_{N_{\text{at}}} / N_{\text{at}}$.

The grand canonical partition function is therefore

$$\begin{aligned} \mathcal{Z}_N(\beta) &= \sum_{\{n_j\}} e^{-\beta \sum_{j=1}^{+\infty} j \delta E_{N_{\text{at}}} n_j + \beta \mu \sum_{j=1}^{+\infty} n_j} = \sum_{\{n_j\}} \prod_{j=1}^{+\infty} e^{-\beta j \delta E_{N_{\text{at}}} n_j + \beta \mu n_j} = \\ &= \prod_{j=1}^{+\infty} \sum_{n=0,1} e^{-\beta j \delta E_{N_{\text{at}}} n_j + \beta \mu n_j} = \prod_{j=1}^{+\infty} (1 + e^{-\beta j \delta E_{N_{\text{at}}} + \beta \mu}) . \end{aligned} \quad (\text{S1})$$

The grand potential is given by

$$\Phi_G = -\frac{1}{\beta N_{\text{at}}} \sum_{j=1}^{+\infty} \ln(1 + e^{-\beta j \delta E_{N_{\text{at}}} + \beta \mu}) = -\frac{1}{\beta N_{\text{at}} \delta E_{N_{\text{at}}}} \sum_{j=1}^{+\infty} \ln(1 + e^{-\beta j \delta E_{N_{\text{at}}} + \beta \mu}) \delta E_{N_{\text{at}}} \quad (\text{S2})$$

and in the continuous limit $N_{\text{at}} \rightarrow \infty$ one obtains that

$$\Phi_G = -\frac{\rho}{\beta} \int_0^{+\infty} \ln(1 + e^{-\beta E + \beta \mu}) dE = \frac{\rho \text{Li}_2[-e^{\beta \mu}]}{\beta^2}, \quad (\text{S3})$$

where Li_2 is the polylogarithm (also known as Jonquière's function) of order 2.

From the grand potential it is possible to calculate the average number of fermions $\langle N \rangle$ and the average energy $\langle E \rangle$ at a given inverse temperature β and chemical potential μ . In the thermodynamical limit $\langle N \rangle = N$ and $\langle E \rangle = E$. Therefore we can write

$$\begin{aligned} N &= \int_0^{+\infty} \frac{\rho}{1 + e^{\beta E - \beta \mu}} dE = \frac{\rho \ln[1 + e^{\beta \mu}]}{\beta} \\ E &= \int_0^{+\infty} \frac{\rho E}{1 + e^{\beta E - \beta \mu}} dE = -\frac{\rho \text{Li}_2[-e^{\beta \mu}]}{\beta^2}. \end{aligned} \quad (\text{S4})$$

We now address the case $1/\beta \ll \mu$, which means that we focus on the case for which the bottom of the band does not play a role. As stated above, this lower bound was included only to ensure a finite value of the integrals, leading to an easier mathematical treatment. It can be easily shown that

$$\begin{aligned} N &\underset{1/\beta \ll \mu}{\approx} \rho \mu \\ E &\underset{1/\beta \ll \mu}{\approx} \frac{\rho \mu^2}{2} + \frac{\pi^2 \rho}{6\beta^2} = E_0 + \frac{\pi^2 \rho}{6\beta^2} \\ \Phi_G &\underset{1/\beta \ll \mu}{\approx} -\frac{\rho \mu^2}{2} - \frac{\pi^2 \rho}{6\beta^2} = -E_0 - \frac{\pi^2 \rho}{6\beta^2} \end{aligned} \quad (\text{S5})$$

where we have named the minimum energy at zero temperature $E_0 \equiv \rho \mu^2 / 2$. We can finally focus on the entropy $S = \beta(-\Phi_G + E - \mu N)$, which can be expressed as

$$S \approx \sqrt{\frac{2\pi^2 \rho (E - E_0)}{3}}. \quad (\text{S6})$$

Although we showed this result for a constant density of states, it holds more generally in the limit where the degenerate gas approximation holds. This is the case when the excitation energy is small compared to the bandwidth, but large compared to the level spacing around the Fermi level. In the case of a slowly varying density of states we can approximate the entropy by:

$$S \approx \sqrt{\frac{2\pi^2 \bar{\rho} (E - E_0)}{3}}, \quad (\text{S7})$$

where $\bar{\rho}$ is an average of the density of states over an energy range comparable to $E - E_0$ and includes the behaviour of both the spin up and spin down channels.

In the main article we discuss the number of ways \mathcal{N} to arrange the electronic excitations in the limit of a large number of atoms. In this limit \mathcal{N} is proportional to $(e^S)^{N_{\text{at}}}$. In the situation sketched in the main article, the minimum energy E_0 of the system is determined by the magnetic configuration, and is denoted as $E_{\text{min}}[(\mathbf{m}_i)]$. The total energy of the system is denoted as E_{tot} . This leads to the number of microstates reported in Eq. 1 of the main paper.

$$\mathcal{N} \propto e^{N_{\text{at}} \sqrt{\bar{\rho}[(\mathbf{m}_i)] (E_{\text{tot}} - E_{\text{min}}[(\mathbf{m}_i)])}} \quad (\text{S8})$$

where the average density of states $\bar{\rho}[(\mathbf{m}_i)]$ depends in principle on the magnetic configuration, in practice however the dependence turns out to be rather weak.

For the system under investigation (Fe), the density of states $\rho[(\mathbf{m}_i)]$ for the ferromagnetic configurations with increased and decreased local moments can be computed directly through constrained density functional theory (DFT) [50], where the constraint is given by fixed spin moments (\mathbf{m}_i) . In our calculations (see below for additional details) we find (data not shown) that the dependence of $\bar{\rho}[(\mathbf{m}_i)]$ on (\mathbf{m}_i) is rather weak, and can in first approximation be ignored. Notice that even when a change of the magnetic configuration is so strong to move bands across the Fermi level the effect on $\bar{\rho}[(\mathbf{m}_i)]$ is weak, since the bands which were available for electronic excitations become available for holes excitations, and viceversa. The same argument is valid when considering the different spin channels. Assuming that $\bar{\rho}[(\mathbf{m}_i)]$ is approximately constant, maximizing the product $\bar{\rho}[(\mathbf{m}_i)] (E_{\text{tot}} - E_{\text{min}}[(\mathbf{m}_i)])$ implies minimizing $E_{\text{min}}[(\mathbf{m}_i)]$, which is instead strongly dependent on the magnetic configuration. Neglecting the change of $\bar{\rho}[(\mathbf{m}_i)]$ becomes a better and better approximation the smaller $(E_{\text{tot}} - E_{\text{min}}[(\mathbf{m}_i)])$ is, compared to the variations of $E_{\text{min}}[(\mathbf{m}_i)]$. For very strong excitations a more accurate description is needed. Notice how in this limit the most probable magnetic configuration will be independent of the total energy E_{tot} deposited by the laser.

ROLE OF ELECTRON-PHONON SCATTERING

In the main text we have assumed for simplicity that electron-phonon scattering is negligible. However its inclusion is straightforward, and does not change anything in our analysis. Again we assume that the spin-flip scattering events are not very frequent for the time scale of the equilibration [28]. Under this assumption, the electron-phonon interaction will make the electronic system behave according to the canonical statistics and not to the microcanonical statistics, which is used in the main paper. The constraint that the total magnetic moment remains fixed still holds. The treatment in the article can therefore be applied as it is by using the canonical statistics. The only consequence is that the averages must be evaluated on all the microstates with arbitrary total energy E_{tot} but weighted by the factor $\exp[-\beta E_{\text{tot}}]$. It means that for each magnetic configuration the total number of ways \mathcal{N}_C to arrange electronic excitations in the canonical ensemble becomes

$$\mathcal{N}_C \propto \int_{E_{\text{min}}[(\mathbf{m}_i)]}^{\infty} e^{-\beta E_{\text{tot}}} e^{N_{\text{at}} \sqrt{\bar{\rho}[(\mathbf{m}_i)] (E_{\text{tot}} - E_{\text{min}}[(\mathbf{m}_i)])}} dE_{\text{tot}}. \quad (\text{S9})$$

It is evident that the magnetic configuration with the lowest $E_{\text{min}}[(\mathbf{m}_i)]$ is even more favoured than in the micro-canonical case.

COMPUTATIONAL DETAILS

For this work we performed density functional theory (DFT) calculations, using the full-potential linearized augmented plane wave (FP-LAPW) method ELK [51]. The calculations were done for body centered cubic (bcc) Fe using the experimental lattice parameter of 5.43 a.u. We addressed the ferromagnetic phase with a constrained total spin moment [50], where the magnetization axis was chosen to be along (100), i.e. the easy axis of Fe. The exchange-correlation functional used in DFT was the generalized-gradient approximation (GGA) by Perdew-Burke-Ernzerhof [52]. The Brillouin zone was sampled with an equally spaced grid using 30 kpoints in each direction which gave 3504 kpoints in the irreducible wedge. The muffin tin radius of the Fe spheres was set to 2.0 a.u. The basis for the valence electrons included 4s, 4p and 3d derived states.

In order to evaluate the optical response, 3s and 3p states were added to the valence states. Spin-orbit coupling, which induces the splitting between the $3p_{1/2}$ and $3p_{3/2}$ states, was also taken into account, again with the magnetization along the easy axis. Moreover the number of empty states was converged (to a value of 40) to correctly describe

the continuum of absorbing states above the Fermi level. The optical conductivity tensor was computed within linear response theory and only direct interband transitions were taken into account [55]. For the configuration with reduced magnetization, we can assume with good approximation that the local electronic structure is not modified by the formation of spin waves with a small \mathbf{q} . The dielectric response can therefore be computed as an average of dielectric responses of bulk systems with a rotating magnetization axis, as described below.

DIELECTRIC TENSORS

In the case of decreased magnetization the dielectric tensors of Fig. 5 of the main article have been computed by employing two approximations. They come from the two assumptions that 1) long wavelength tilting of the magnetic moments have a negligible influence on the local dielectric tensor and that 2) the magnetic anisotropy is negligible. The first approximation implies that the dielectric response of the material can be computed as an average of local responses. These can be evaluated directly from ferromagnetic bulk Fe with a magnetization that is aligned with the local magnetic moments. The longer the wavelength of the tilting of the magnetic moments is, the better this approximation holds. According to the second approximation the dielectric response of a material whose magnetization is oriented towards a direction that is not the easy axis is negligibly different from the response obtained by simply rotating the dielectric tensor. The error produced by this approximation is related to the anisotropy of the material, and is fully justified for Fe as the magnetic anisotropy energy is of order of μeV .

In case of decreased magnetization our model predicts that the local magnetic moments are tilted by an angle θ from the z axis in random directions in the xy plane. Therefore, we can compute the average dielectric tensor for reduced magnetization as an average of the rotated dielectric tensors. We first tilt our magnetic moment over an angle θ from the z axis. Second, we rotate our magnetic moment around the z axis with an angle ϕ and average over all angles $0 \leq \phi \leq 2\pi$.

The rotation matrix over θ is given by

$$R(\theta) = \begin{pmatrix} \cos \theta & 0 & \sin \theta \\ 0 & 1 & 0 \\ -\sin \theta & 0 & \cos \theta \end{pmatrix} \quad (\text{S10})$$

while the rotation over ϕ is given by

$$R(\phi) = \begin{pmatrix} \cos \phi & -\sin \phi & 0 \\ \sin \phi & \cos \phi & 0 \\ 0 & 0 & 1 \end{pmatrix} \quad (\text{S11})$$

The tilting of the dielectric tensor by an angle θ and the following average over ϕ can now be rewritten as :

$$\begin{aligned} \langle \epsilon \rangle &= \frac{1}{2\pi} \int_0^{2\pi} R(\phi) R(\theta) \epsilon R^{-1}(\theta) R^{-1}(\phi) d\phi \\ &= \begin{pmatrix} \frac{1}{4}(\epsilon_{xx} + 2\epsilon_{yy} + \epsilon_{zz} + (\epsilon_{xx} - \epsilon_{zz}) \cos 2\theta) & \epsilon_{xy} \cos \theta - \epsilon_{yz} \sin \theta & 0 \\ -\epsilon_{xy} \cos \theta + \epsilon_{yz} \sin \theta & \frac{1}{4}(\epsilon_{xx} + 2\epsilon_{yy} + \epsilon_{zz} + (\epsilon_{xx} - \epsilon_{zz}) \cos 2\theta) & 0 \\ 0 & 0 & \epsilon_{xx} \sin^2 \theta + \epsilon_{zz} \cos^2 \theta \end{pmatrix} \end{aligned} \quad (\text{S12})$$

where the symbol $\langle \rangle$ reminds that it is a spatial average. For the case of Fe, where $\epsilon_{xz} = \epsilon_{zx} = \epsilon_{yz} = \epsilon_{zy} = 0$ and $\epsilon_{xx} = \epsilon_{yy} \approx \epsilon_{zz}$, this simplifies to:

$$\langle \epsilon \rangle \approx \begin{pmatrix} \epsilon_{xx} & \epsilon_{xy} \cos \theta & 0 \\ -\epsilon_{xy} \cos \theta & \epsilon_{xx} & 0 \\ 0 & 0 & \epsilon_{xx} \end{pmatrix} \quad (\text{S13})$$

Finally, the off-diagonal terms of the dielectric tensor for both decreased and increased magnetization are shown in Fig. S1. This is simply a more extended version of Fig. 5 of the main paper. For sake of completeness we also report in Fig. S2 the diagonal terms of the dielectric tensor, for increased magnetization only. Notice that also here the only changes are visible below the main Fe peak, in the region highlighted within the red box. As expected from Eq. S13, the diagonal components do not change much in case of decreased magnetization, and are therefore not shown.

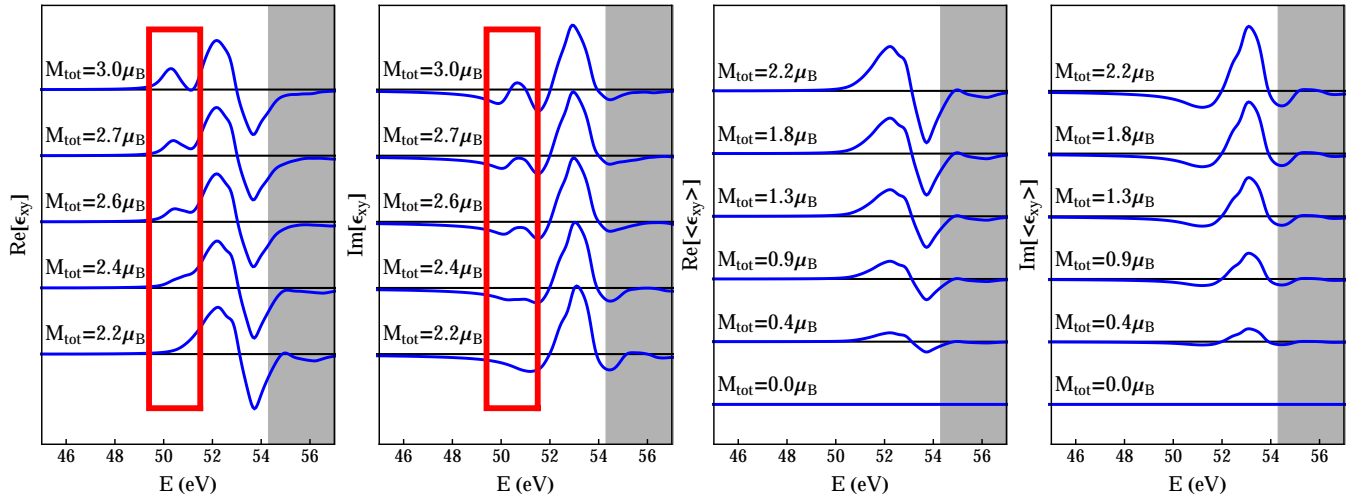


FIG. S1. [Colour online] Real and imaginary part of the off-diagonal term ϵ_{xy} of the dielectric tensor for the case of increased and decreased magnetization. For increased magnetization a shoulder in the lower part of the main Fe peak is formed, as highlighted within the red box.

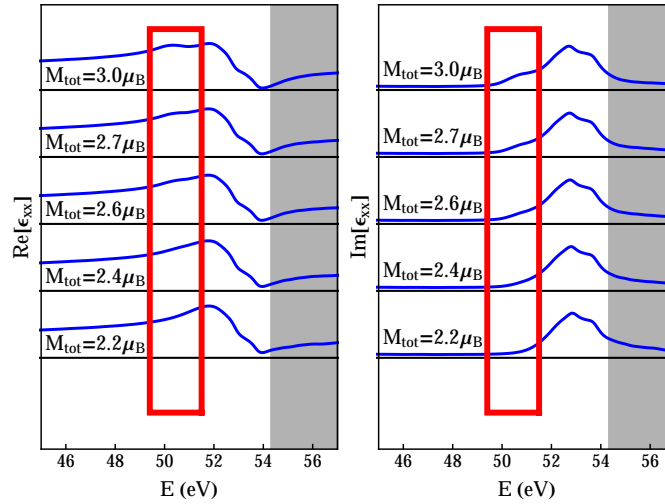


FIG. S2. [Colour online] Real and imaginary part of the diagonal term ϵ_{xx} of the dielectric tensor for the case of increased magnetization. The red box individuates the region where a shoulder in the Fe main peak forms in the off-diagonal term ϵ_{xy} , as reported in in Fig. S1. Notice that also in these curves the only noticeable changes happen below 52 eV.